Acta Pharmaceutica Sinica B 2024;14(3):1428−1440

Chinese Pharmaceutical Association
Institute of Materia Medica, Chinese Academy of Medical Sciences

Acta Pharmaceutica Sinica B

www.elsevier.com/locate/apsb
www.sciencedirect.com

ORIGINAL ARTICLE

# Photo-induced crosslinked and anti-PD-L1 peptide incorporated liposomes to promote PD-L1 multivalent binding for effective immune checkpoint blockade therapy

**Youngjoo Lee[a,b,†], Sukyung Song[c,†], Suah Yang[a,b], Jinseong Kim[a,b], Yujeong Moon[a,d], Nayeon Shim[c], Hong Yeol Yoon[b], Sehoon Kim[a,b], Man Kyu Shim[b,*], Kwangmeyung Kim[c,*]**

[a]*KU-KIST Graduate School of Converging Science and Technology, Korea University, Seoul 02841, Republic of Korea*
[b]*Medicinal Materials Research Center, Biomedical Research Division, Korea Institute of Science and Technology (KIST), Seoul 02792, Republic of Korea*
[c]*College of Pharmacy, Graduate School of Pharmaceutical Sciences, Ewha Womans University, Seoul 03760, Republic of Korea*
[d]*Department of Bioengineering, Korea University, Seoul 02841, Republic of Korea*

Received 9 June 2023; received in revised form 31 July 2023; accepted 15 August 2023

**KEY WORDS**

Cancer immunotherapy;
Immune checkpoint blockade;
PEGylated liposome;
Crosslinked lipid nanoparticles;
Anti-PD-L1 peptide;
Tumor-targeting;
PD-L1 multivalent binding;

**Abstract** Immune checkpoint blockade (ICB) therapy targeting PD-L1 *via* monoclonal antibody (mAb) has shown extensive clinical benefits in the diverse types of advanced malignancies. However, most patients are completely refractory to ICB therapy owing to the PD-L1 recycling mechanism. Herein, we propose photo-induced crosslinked and anti-PD-L1 peptide incorporated liposomes (immune checkpoint blockade liposomes; ICB-LPs) to promote PD-L1 multivalent binding for inducing lysosomal degradation of PD-L1 in tumor cells. The ICB-LPs are prepared by formulation of $DC_{8,9}PC$ with photo-polymerized diacetylenic moiety, 1,2-dipalmitoylphosphatidylcholine (DPPC) and anti-PD-L1 peptide (D-form NYSKPTDRQYHF)-conjugated DSPE-$PEG_{2k}$ (anti-PD-L1-DSPE-$PEG_{2k}$) in a molar ratio of 45:45:10, followed by cross-linking of liposomal bilayer upon UV irradiation. The 10 mol% anti-PD-L1-DSPE-$PEG_{2k}$ incorporated ICB-LPs have a nano-sized lipid bilayer structure with an average diameter of 137.7 ± 1.04 nm, showing a high stability in serum condition. Importantly, the ICB-LPs

*Corresponding authors.
E-mail addresses: mks@kist.re.kr (Man Kyu Shim), kimkm@ewha.ac.kr (Kwangmeyung Kim).
[†]These authors made equal contributions to this work.
Peer review under the responsibility of Chinese Pharmaceutical Association and Institute of Materia Medica, Chinese Academy of Medical Sciences.

https://doi.org/10.1016/j.apsb.2023.09.007

Lysosomal PD-L1 degradation

efficiently promote the multivalent binding with PD-L1 on the tumor cell membrane, which are endocytosed with aim to deliver PD-L1 to the lysosomes, wherein the durable PD-L1 degradation is observed for 72 h, in contrast to anti PD-L1 mAbs showing the rapid PD-L1 recycling within 9 h. The *in vitro* co-culture experiments with $CD8^+$ T cells show that ICB-LPs effectively enhance the T cell-mediated anti-tumor immune responses against tumor cells by blocking the PD-L1/PD-1 axis. When ICB-LPs are intravenously injected into colon tumor-bearing mice, they efficiently accumulate within the targeted tumor tissues *via* both passive and active tumor targeting, inducing a potent T cell-mediated antitumor immune response by effective and durable PD-L1 degradation. Collectively, this study demonstrates the superior antitumor efficacy of crosslinked and anti-PD-L1 peptide incorporated liposome formulation that promotes PD-L1 multivalent binding for trafficking of PD-L1 toward the lysosomes instead of the recycling endosomes.



## 1. Introduction

Cytotoxic T lymphocytes (CTLs) recognize the major histocompatibility complexes (MHCs) on target tumor cells *via* T-cell receptors (TCRs) to eradicate the tumors[1]. However, several co-inhibitory or co-stimulatory ligands and its receptors, known as immune checkpoints, predominantly modulate the interaction between CTLs and tumor cells[2]. In particular, the interaction between programmed death-ligand 1 (PD-L1) on tumor cells and programmed cell death protein 1 (PD-1) on T cells promotes immune escape mechanism in tumor cells and inhibits activation, expansion and effector functions of CTLs[3]. The PD-L1 expression in the tumor cells can be upregulated by inflammatory cytokines of interferon-γ (IFN-γ) secreted from T cells within the tumor microenvironment as well as also driven by intrinsic amplification mechanisms of the PD-L1 locus and structural variation of the PD-L1 gene[4,5]. Hence, the immune checkpoint blockade (ICB) therapy targeting PD-L1 on the tumor cell surface *via* monoclonal antibodies (mAbs) has emerged as a remarkable therapeutic approach, which has shown extensive clinical benefits in the diverse types of advanced malignancies[6,7]. However, although PD-L1 blockade has significantly improved the patient's clinical outcomes, only a less than 20% of patients show a durable response, and many patients are completely refractory to ICB therapy owing to intrinsic resistance mechanisms[8].

Intrinsic resistance of tumor cells to ICB therapy targeting PD-L1 can be attributable to a recycling mechanism by which endocytosed PD-L1 after conformational blockade with PD-L1 mAbs is actively recycled back to the cell membranes[9]. This is because the complexes of PD-L1/PD-L1 mAbs are prone to enter into recycling endosomes instead of lysosomes following endocytosis and thereby prevent the lysosomal degradation of PD-L1[10]. This PD-L1 recycling mechanism considerably reduces the response rate and efficacy of ICB therapy, thus tremendous efforts have been made to analyze the regulatory process of PD-L1. Recently, several factors that play a crucial role in subcellular PD-L1 recycling have been reported: (i) chemokine-like factor-like MARVEL transmembrane domain-containing family member 6 (CMTM6) maintains PD-L1 at cell surface and sort it to the recycling endosomes, thereby preventing the lysosomal degradation of PD-L1; (ii) trafficking protein particle subunit 4 (TRAPPC4), a key subunit of TRAPP complex, maintains the expression of PD-L1 by coordinating RAB11-mediated PD-L1 recycling and preventing lysosomal PD-L1 degradation, ultimately promoting immune escape mechanism in the tumor cells; and (iii) huntingtin interacting protein 1-related (HIP1R) protein, which physically interacts with PD-L1, delivers PD-L1 to the lysosomes through lysosomal sorting signals, resulting in PD-L1 degradation to trigger T cell-mediated antitumor immune responses[10–12]. These findings suggest that subcellular trafficking of PD-L1 to the lysosomes can be a potential method to improve the response rate and efficacy of ICB therapy, but there has been little study on therapeutic approaches.

Importantly, promoting multivalent binding of PD-L1 and its ligands can efficiently lead to the internalization and lysosome delivery of PD-L1. It has been known that the multivalent binding complexes of surface receptors and ligands alter the endocytosis pathway and subcellular trafficking, resulting in internalization to the lysosomes[13]; these aberrant lysosomal deliveries have been observed for many receptors, such as epidermal growth factor receptor (EGFR), acetylcholine receptors (AChR) and FcRn receptors[14–16]. As an approach for lysosomal delivery of PD-L1, the 2-hydroxypropyl methacrylamide (HPMA) polymers modified with a number of anti-PD-L1 peptide promoted PD-L1 multivalent binding on the tumor cell surface and trafficked PD-L1 to the lysosomes instead of recycling endosomes, thus inhibiting subcellular PD-L1 recycling mechanism[9]. In addition, nano-sized dendrimers containing multiple PD-L1 mAbs significantly improved the efficiency of ICB therapy by disrupting interaction between PD-L1 on tumor cells and PD-1 on T cells *via* multivalent binding-mediated lysosomal PD-L1 degradation[17]. Our previous study optimized the density of anti-PD-L1 peptides on liposome surface to facilitate a multivalent binding for lysosomal delivery of PD-L1 *via* the clinically-used liposome formulation[18]. In contrast to PD-L1 mAb-treated tumor cells that showed rapid PD-L1 recycling within 24 h of treatment, PEGylated liposomes incorporating 10 mol% anti-PD-L1 peptide effectively down-regulated the PD-L1 expression in the tumor cells for 3 days *via* multivalent binding-mediated lysosomal delivery of PD-L1 for its effective and durable degradation.

Herein, we propose photo-induced crosslinked and anti-PD-L1 peptide incorporated liposomes (immune checkpoint blockade liposomes, ICB-LPs) to promote PD-L1 multivalent binding for internalization and lysosomal delivery of PD-L1 in targeted tumor cells. The ICB-LPs are prepared by formulation of 1,2-bis(10,12-tricosadiynoyl)-*sn*-glycero-3-phosphocholine ($DC_{8,9}PC$) with

photo-polymerized diacetylenic moiety, 1,2-dipalmitoylphosphatidylcholine (DPPC) and anti-PD-L1 peptide (D-form NYSKPTDRQYHF)-conjugated 1,2-distearoyl-*sn*-glycero-3-phosphoethanolamine-*N*-[methoxy (polyethylene glycol)2k] (anti-PD-L1-DSPE-$PEG_{2k}$) in a molar ratio of 45:45:10. As expected, $DC_{8,9}PC$ is a type of phospholipid, which can promote intermolecular crosslinking within the liposomal bilayers upon ultra-violet (UV) irradiation (Scheme 1A)[19]. The 10 mol% of anti-PD-L1-DSPE-$PEG_{2k}$ is incorporated into ICB-LPs. This is because approximately 10 mol% incorporation of PEGylated lipids promotes PD-L1 multivalent binding based on previous study that demonstrated optimal density of anti-PD-L1 peptides on the liposome surface[18]. After UV irradiation, the crosslinked ICB-LPs show a superior serum stability in the blood flow, contributing to enhanced PD-L1 target accessibility by passive tumor accumulation owing to the enhanced permeability and retention (EPR) effect and the tumor targeting of ICB-LPs is further enhanced by PD-L1 receptor-mediated active targeting mechanism at targeted PD-1 overexpressed tumor tissues (Scheme 1B)[20]. In particular, ICB-LPs are able to promote multivalent binding with the targeted PD-L1 on the tumor cell surface, which efficiently internalizes in the cells *via* nanoparticle-derived endocytosis with aim to deliver PD-L1 to the lysosomes instead of recycling endosomes (Scheme 1C). As a result, ICB-LPs significantly decrease the PD-L1 expression in the tumor cells by inducing lysosomal PD-L1 degradation, resulting in enhanced CTL-mediated antitumor immune responses. In contrast, anti-PD-L1 mAb-induced PD-L1 blockade prone to be recycled back to the membranes because of their intrinsic endocytosis pathway targeting recycling endosomes, thereby reducing CTL activity (Scheme 1D). In this study, the optimal ICB-LPs were prepared by crosslinking of 10 mol% of anti-PD-L1-DSPE-$PEG_{2k}$ incorporated liposomes upon UV irradiation and their physiochemical properties were evaluated in physiological condition. In cell culture system, the effects to promote PD-L1 multivalent binding for internalization and lysosomal PD-L1 delivery by ICB-LPs are directly visualized in the mGFP-tagged PD-L1-expressing tumor cells. In addition, the efficient lysosomal PD-L1 degradation by ICB-LPs is assessed *in vitro* co-culture experiments with $CD8^+$ T cells. Finally, a potent antitumor immune response induced by a significant lysosomal PD-L1 degradation is evaluated in the colon tumor-bearing mice.

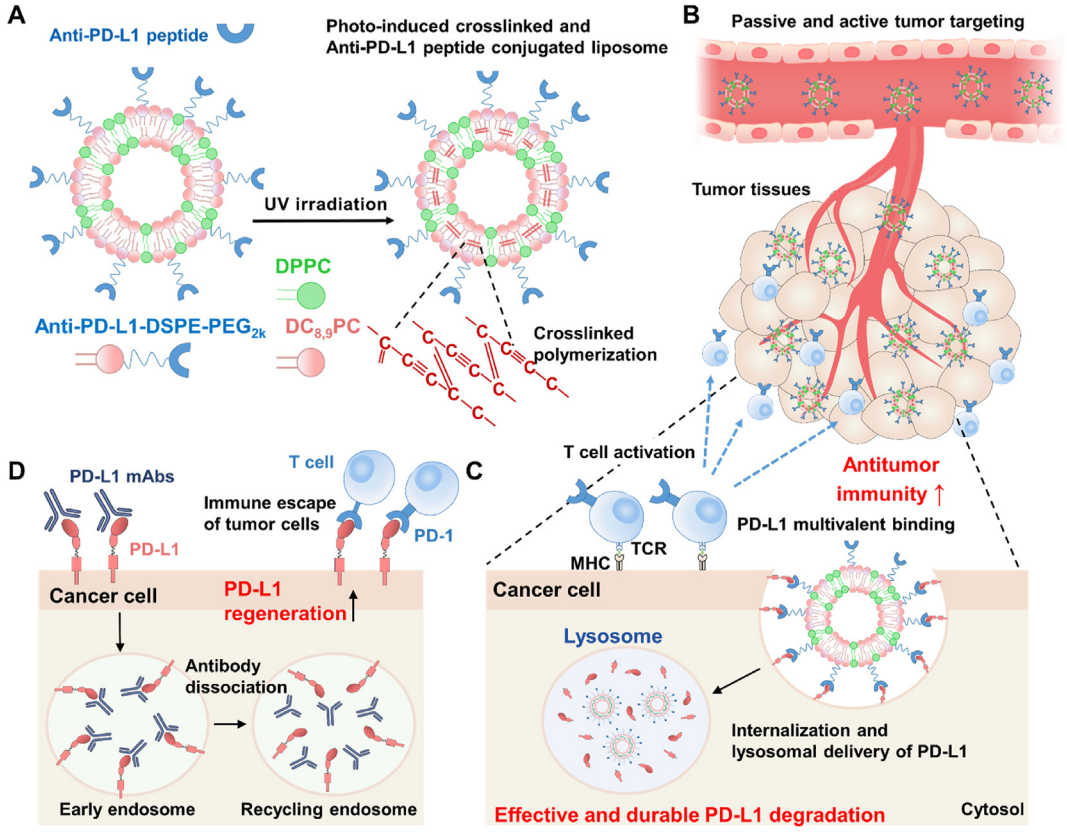


**Scheme 1** PD-L1 multivalent binding of ICB-$LPs^{+UV}$ for effective immune checkpoint blockade therapy. (A) The ICB-LPs are prepared by formulation of $DC_{8,9}PC$, DPPC and anti-PD-L1-DSPE-$PEG_{2k}$, which can promote intermolecular crosslinking within the liposomal bilayers upon UV irradiation. (B) ICB-$LPs^{+UV}$ highly accumulates within the tumor tissues *via* EPR effect and PD-L1 receptor-mediated active targeting mechanisms. (C) ICB-$LPs^{+UV}$ efficiently promotes multivalent binding with the PD-L1 on the tumor cell surface, which efficiently internalizes in the cells *via* nanoparticle-derived endocytosis with aim to deliver PD-L1 to the lysosomes. As a result of effective lysosomal PD-L1 degradation, a potent CTL-mediated antitumor immunity is induced. (D) In contrast, PD-L1 mAb-induced PD-L1 blockade prone to be recycled back to the membranes because of their intrinsic endocytosis pathway targeting recycling endosomes, thereby reducing CTL activity.

## 2. Materials and methods

### 2.1. Reagents

1,2-Distearoyl-*sn*-glycero-3-phosphoethanolamine-*N*-[methoxy (polyethylene glycol)$_{2k}$] (DSPE-PEG$_{2k}$), 1,2-distearoyl-*sn*-glycero-3-phospho-ethanolamine-*N*-[amino (polyethylene glycol)$_{2k}$]-amine (DSPE-PEG-NH$_2$) and 1,2-bis(10,12-tricosadiynoyl)-*sn*-glycero-3-phosphocholine (DC$_{8,9}$PC) were purchased from Avanti Polar Lipids Inc. (Alabaster, AL, USA). Bicylco [6.1.0]nonyne *N*-hydroxysuccinimide ester II (BCN−NHS) was purchased from Berry & Associates (Dexter, MI, USA). Flamma 648 Azide (cat# PWZ1215) was purchased from BioActs (Incheon, Republic of Korea). *N*-terminal azidoacetylated anti-PD-L1 D-peptide ($N_3$-Asn-Tyr-Ser-Lys-Pro-Thr-Asp-Arg-Gln-Tyr-His-Phe-COOH) was synthesized by Peptron (Daejeon, Republic of Korea). Anti-mouse calreticulin antibody was purchased from Abcam (Hanam, Republic of Korea). Fluorescent dye-conjugated antibodies against mouse CD45.2, mouse CD3, mouse CD8α, mouse PD-L1, mouse CD4, mouse CD25, mouse granzyme B and red blood cell lysis buffer were purchased from BioLegend (San Diego, CA, USA). IFN-γ Quantikine ELISA Kit and CD8$^+$ T cell column kit were purchased from R&D system (Minneapolis, MN, USA). Tumor Dissociation Kit and T Cell Activation/Expansion Kit were purchased from Miltenyi Biotechnology (Bergisch Gladbach, North Rhine-Westphalia, Germany). Interferon gamma (IFN-γ) and recombinant mouse interleukin-2 (IL-2) were purchased from PeproTech (Seoul, Republic of Korea). Human Tagged ORF Clone Lentiviral Particle (mGFP-tagged PD-L1) was purchased from ORIGENE (Rockville, MD, USA). Anti-PD-L1 antibody (B7−H1) was purchased from BioXCell.

### 2.2. Preparation and characterization of ICB-LPs

First, the anti-PD-L1-DSPE-PEG$_{2k}$ was synthesized *via* a two-step chemical reaction. Briefly, 1,2-distearoyl-*sn*-glycero-3-phosphoethanolamine-*N*-[amino (polyethylene glycol)$_{2k}$]-amine (DSPE-PEG$_{2k}$-NH$_2$; 216 mg, 78 mmol) and bicylco [6.1.0]nonyne *N*-hydroxysuccinimide ester II (BCN−NHS; 50 mg, 94 mmol) were dissolved in a methanol/chloroform mixture (1:3, *v*/*v*) for 12 h at 37 °C. Then, the unreacted chemical was removed through a dialysis membrane (MWCO: 500−1000 Da) in distilled water for 48 h, and the solution was lyophilized for 72 h to yield BCN-DSPE-PEG$_{2k}$. Afterwards, BCN-DSPE-PEG$_{2k}$ (230 mg, 72 mmol) and *N*-azidoacetyl anti-PD-L1 D-peptide ($N_3$-NYSKPTDRQYHF-COOH; 180 mg, 132 mmol) were reacted within a mixture of distilled water and acetonitrile (1:4, *v*/*v*) *via* click chemistry reaction. After 48 h of reaction, the unreacted chemical was removed through a dialysis membrane (MWCO: 3500 Da) in distilled water, followed by lyophilization for 72 h to yield anti-PD-L1-DSPE-PEG$_{2k}$. Next, liposomes were prepared *via* simple film casting method. Briefly, phospholipids (DC$_{8,9}$PC), DPPC and anti-PD-L1-DSPE-PEG$_{2k}$ were dissolved in chloroform at a specific molar ratio of 45/45/10 mol%. Then, the solvents evaporated under a gentle stream with argon at 60 °C until uniform lipid films were formed, followed by hydration in PBS for 30 min at 40 °C. Finally, the hydrated liposomes were sonicated using a probe-type sonifier (Ultrasonic Processor, Cole−Parmer Inst. Co., East Bunker, IL, USA) for 5 min and subsequently extruded for 20 cycles using a hand-held extruder with two stacks of 200 nm polycarbonate membranes. For the crosslinking of lipid bilayers of liposomes, the samples were exposed to the UV irradiation with power of 115 V, 60 Hz-254 nm for 20 min, resulting in ICB-LPs. The structural morphology and size distribution of ICB-LPs were confirmed using CryoTEM (200 kV at −170 °C; Tecnai F20, FEI, Netherlands) and dynamic light scattering (DLS; Zetasizer Nano ZS, Malvern Instruments, Worcestershire, UK), respectively. To verify the PD-L1 multivalent binding of each ICB-LPs$^{+UV}$, biolayer interferometry (BLI) was performed by using a BLItz system (ForteBio, CA, USA). For this analysis, recombinant mouse PD-L1 (50 μg/mL) was immobilized on the Protein A biosensor (ForteBio). Then, biosensors were washed with kinetic buffers and reacted with D-form NYSKPTDRQYHF, ICB-LPs$^{+/-UV}$ incorporating 5 or 10 mol% of anti-PD-L1-DSPE-PEG$_{2k}$, wherein each sample has the same anti-PD-L1 peptide concentration of 0.067 μmol. As a control, 0.067 μmol of PD-L1 mAbs was used in biolayer interferometry (BLI) experiment.

### 2.3. Cytotoxicity assays

The cytotoxicity of PEG-LPs, ICB-LPs$^{-UV}$ or ICB-LPs$^{+UV}$ was assessed *via* the Cell Counting Kit-8 (CCK-8) assays. For these analyses, $1 \times 10^6$ CT26 cells were seeded into 96-well cell culture plate. After 24 h of stabilization, the cells were treated with each liposome (0−0.5 mg/mL). After 48 h of incubation, the cells were incubated with cell culture medium containing 10% CCK-8 solution for 30 min. The cell viability was confirmed using a microplate reader at a wavelength of 450 nm (VERSAmaxTM; Molecular Devices Corp., San Jose, CA, USA).

### 2.4. Cellular binding and uptake of ICB-LPs$^{+UV}$

To assess the cellular binding ICB-LPs$^{+UV}$, $1 \times 10^6$ CT26 cells were seeded in the glass-bottom confocal dishes and incubated with PD-L1 mAbs (0.067 μmol), PEG-LPs, ICB-LPs$^{-UV}$ (0.067 μmol based on anti-PD-L1 peptide) or ICB-LPs$^{+UV}$ (0.067 μmol based on anti-PD-L1 peptide) for 1 h at 4 °C. As control experiments, CT26 cells were pre-treated with PD-L1 mAbs or anti-PD-L1 peptide (NYSKPTDRQYHF) for 1 h at 4 °C to quantitatively block the PD-L1 on cell surfaces. The cellular uptake of PD-L1 mAb, ICB-LPs$^{-UV}$ and ICB-LPs$^{+UV}$ was investigated in the CT26 cells after treatment for 0, 3, 6 and 12 h at 37 °C. For the analysis of the levels of PD-L1, mGFP-CT26 cells were treated with PD-L1 mAb, ICB-LPs$^{-UV}$ and ICB-LPs$^{+UV}$ for 0, 3, 6, 9, 24, 48 and 72 h. As a control, PD-L1 expression in the mGFP-CT26 cells pre-treated with chloroquine (100 μmol) for 24 h was assessed after treatment with ICB-LPs$^{-UV}$ and ICB-LPs$^{+UV}$ for 48 h. After treatment, the cells were washed with DPBS, fixed with 4% paraformaldehyde for 10 min, and stained with 4',6-diamidino-2-phenylindole (DAPI) for 15 min. Cellular fluorescence imaging was performed using a Leica TCS SP8 confocal laser-scanning microscope (Leica Microsystems GmbH; Wetzlar, Germany).

### 2.5. Co-culture study

Five-weeks-old male BALB/c mice were purchased from NaraBio Inc. (Gyeonggi-do, Republic of Korea). Mice were bred at the Korea Institute of Science and Technology (KIST) under pathogen-free conditions. All animal experiments were performed in compliance with the relevant laws and institutional guidelines of the Institutional Animal Care and Use Committee (IACUC; approval number 2020-123) of the Korea Institute of Science and

Technology (KIST). The $CD8^+$ T cells were isolated from lymph nodes and spleen of the mice using a $CD8^+$ T cell isolation kits and activated using a T cell activation/expansion kit (Miltenyi Biotechnology, Bergisch Gladbach, North Rhine-Westphalia, Germany). Activated $CD8^+$ T cells were co-cultured with CT26 cells treated with PD-L1 mAb (0.067 μmol), ICB-$LPs^{-UV}$ or ICB-$LPs^{+UV}$ (0.067 μmol based on anti-PD-L1 peptide) for 24 h at 37 °C. Afterwards, IFN-γ in the cell culture medium was measured *via* an IFN-γ ELISA Kit. The viability of CT26 cells after co-culture was also assessed by a CCK-8 assay. The CD107a exposure on the $CD8^+$ T cells was assessed by confirming $CD3^+CD8^+CD107a^+$ cells within the co-cultured cells.

### 2.6. *In vivo biodistribution of ICB-$LPs^{+UV}$ in colon tumor-bearing mice*

First, pharmacokinetics (PK) profiles of DiD-labeled PEG-LPs, ICB-$LPs^{-UV}$ and ICB-$LPs^{+UV}$ (1 mg/kg) were assessed in the BALB/c mice after intravenous injection. At pre-determined times after injection, blood samples were collected from mice *via* cardiac puncture after deep anesthesia, followed by analysis with IVIS Lumina Series III system (PerkinElmer; Waltham, MA, USA). The PK parameters of area under the curves (AUC) and half-life ($t_{1/2}$) were calculated using a Prism9 software (GraphPad, Boston, MA, USA). The *in vivo* tumor targeting and PD-L1 degradation of ICB-$LPs^{+UV}$ were assessed in colon tumor-bearing mice that were prepared by subcutaneous inoculation of $1 \times 10^6$ CT26 cells into the flank. When the tumor volumes were approximately 200 $mm^3$, PEG-LPs, ICB-$LPs^{-UV}$ or ICB-$LPs^{+UV}$ (1 mg/kg) were intravenously injected into the mice. Noninvasive near-infrared fluorescence (NIRF) imaging was performed after 24 h of injection using an IVIS Lumina Series III system (PerkinElmer; Waltham, MA, USA). Then, *ex vivo* NIRF imaging of the major organs and tumor tissues were performed using an IVIS Lumina Series III system, and fluorescence intensities in each tissue were quantified using Living Image software (PerkinElmer, Waltham, MA, USA). Finally, tumor tissues of mice were collected from the mice after 24 h of injection. For the Western blot analyses, tissues were homogenized in the RIPA buffer and centrifuged at 4000 rpm (Combi R515, Hanil, Daejeon, Republic of Korea) for 20 min to remove the debris. After protein quantification with BCA protein assay kit (Thermo Fisher Scientific, USA), the samples were separated by sodium dodecyl sulfate-polyacrylamide (SDS-PAGE) gel electrophoresis and then transferred onto nitrocellulose (NC) membranes. The membrane was incubated with TBS-T containing 5% BSA for 1 h and further incubated with anti-mouse PD-L1 antibody for 24 h at 4 °C. The immunoreactive bands were confirmed *via* enhanced chemiluminescence systems after incubation with HRP-conjugated anti-goat IgG antibody for 2 h at room temperature.

### 2.7. *Antitumor efficacy and immune responses of ICB-$LPs^{+UV}$*

The antitumor efficacy was assessed in the CT26 colon and 4T1 breast tumor-bearing mice. Each tumor model was prepared by subcutaneous inoculation with $1 \times 10^6$ of CT26 of 4T1 cells. The mice were randomly divided into four groups of (i) saline; (ii) PD-L1 mAbs (10 mg/kg); (iii) ICB-$LPs^{-UV}$ (1 mg/kg) and (iv) ICB-$LPs^{+UV}$ (1 mg/kg). The tumor-bearing mice were treated once every three days, and the tumor volumes, calculated as the largest diameter × smallest diameter$^2$ × 0.53, were measured once every two days. The mice with a tumor size of 2000 $mm^3$ or higher were counted as dead. To evaluate the immune responses, the tumor tissues were collected on Day 18 after each treatment, and single cells were isolated from the tissues using a Tumor Dissociation Kit (Miltenyi Biotechnology, Hergisch Gladbach, Germany). The single cells were then incubated with FcBlock for 10 min to avoid non-specific IgG binding. Finally, multiparameter staining was performed for 1 h to assess the quantities of cytotoxic T lymphocytes (CTL; $CD45^+CD3^+CD8^+$), granzyme B (GrzB)-secreting $CD8^+$ T cells ($CD3^+CD8^+GrzB^+$) and regulatory T lymphocytes (Treg; $CD3^+CD4^+CD25^+$) in the tumor tissues.

### 2.8. *Statistics*

The statistical significance between two groups was analyzed using Student's *t*-test. One-way analysis of variance (ANOVA) was performed for comparisons of more than two groups, and multiple comparisons were analyzed using Tukey−Kramer *post-hoc* test. Survival data was plotted as Kaplan−Meier curves and analyzed using log-rank test. Statistical significance was indicated with asterisk ($^*P < 0.05$, $^{**}P < 0.01$, $^{***}P < 0.001$) in the figures.

### 2.9. *Data availability*

All relevant data are available with the article and its supplementary information files, or available the corresponding authors upon reasonable requests.

## 3. Results and discussion

### 3.1. *Preparation and characterization of immune checkpoint blockade liposomes (ICB-LPs)*

First, we prepared photo-induced crosslinked and anti-PD-L1 peptide incorporated liposomes (ICB-LPs), which is constructed with $DC_{8,9}PC$, DPPC and anti-PD-L1-DSPE-$PEG_{2k}$. The anti-PD-L1 D-form peptide that contains azide ($N_3$) group at N-terminus ($N_3$-NYSKPTDRQYHF-COOH) was chemically conjugated with bicyclononyne (BCN)-DSPE-$PEG_{2k}$ *via* copper-free click chemistry reaction to yield anti-PD-L1-DSPE-$PEG_{2k}$, which has a suitable hydrophobic-hydrophilic balance to insert into the liposome formulation (Supporting Information Fig. S1A). Compared to anti-PD-L1 mAb (PD-L1 mAb) structure for ICB therapy, small peptide antagonists have distinct advantages, such as great amenability for chemical synthesis, easy quality control (QC) and mass production, low manufacturing cost, and low immunogenicity[21]. In addition, the anti-PD-L1 peptide, NYSKPTDRQYHF D-peptide, showed the strong biding affinity of 0.51 μmol/L to PD-L1 on tumor cell surface[22]. Successful synthesis of anti-PD-L1-DSPE-$PEG_{2k}$ was confirmed by $^1$H NMR spectrum that shows the both characteristics peaks of hydrocarbons in the lipid (1.4 ppm) and hydroxyl group in serine (S; 9.1 ppm) (Fig. S1B).

In order to prepare ICB-LPs, $DC_{8,9}PC$, DPPC and anti-PD-L1-DSPE-$PEG_{2k}$ were firstly dissolved in chloroform at a specific molar ratio of 45:45:10 mol%and the solvent was evaporated to make a uniform lipid film and then the lipid film was hydrated in PBS for 30 min at 40 °C (Fig. 1A). Then, the multi-lamellar vesicles were further sonicated for 5 min and extruded for 20 cycles with 200 nm of polycarbonate membrane. The freshly prepared liposomes had a homogeneous lipid structure with an average size of 134.3 ± 4.82 nm (Supporting Information

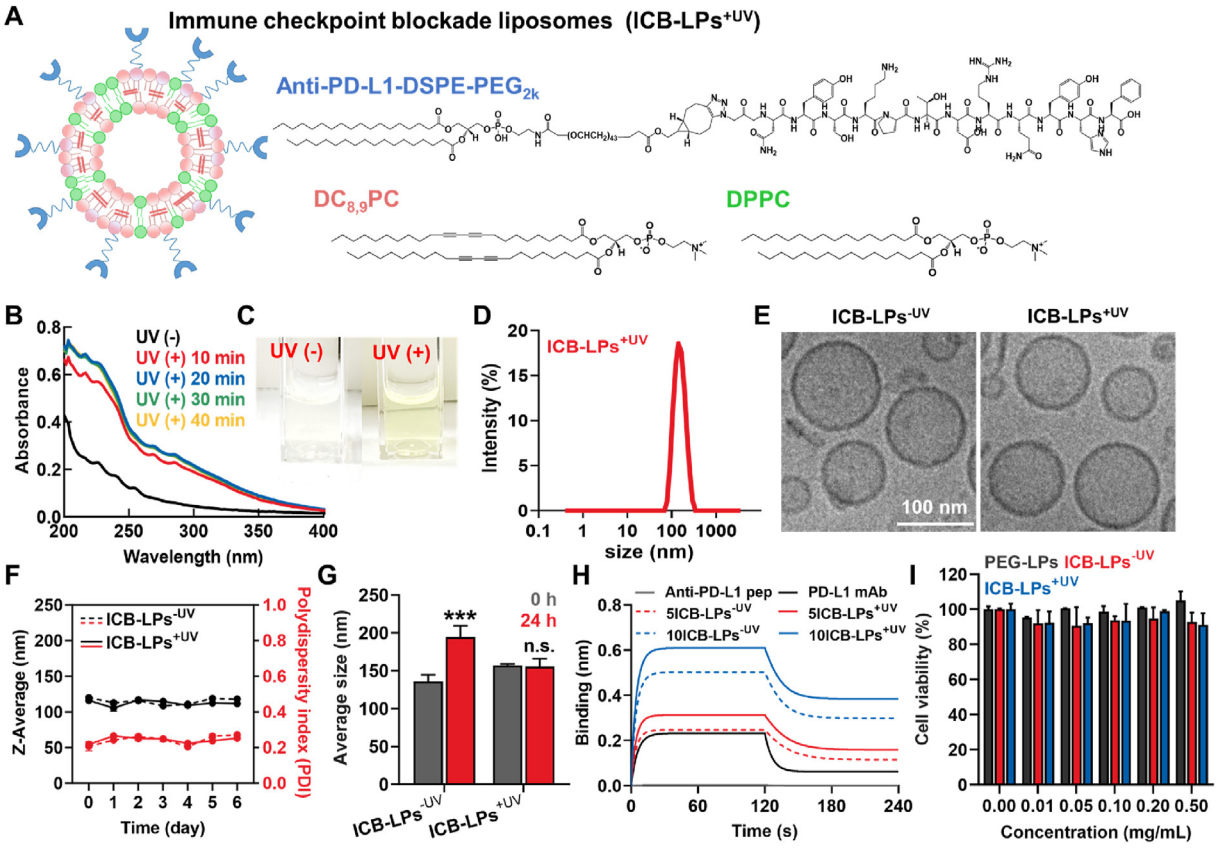


**Figure 1** Preparation and Characterization of ICB-LPs$^{+UV}$. (A) The detail composition of ICB-LPs$^{+UV}$. The ICB-LPs are prepared by formulation of $DC_{8,9}PC$, DPPC anti-PD-L1-DSPE-$PEG_{2k}$ in a molar ratio of 45:45:10. (B) UV−Vis spectrum of ICB-LPs upon different time (10, 20, 30 and 40 min) of UV exposure. (C) Optical images of ICB-LPs before and 10 min after UV irradiation. (D) Size distribution of ICB-LPs$^{+UV}$ in saline (1 mg/mL). (E) Cryo-TEM images of ICB-LPs$^{-UV}$ and ICB-LPs$^{+UV}$ in distilled water (1 mg/mL). (F) The size and polydispersity index (PDI) of ICB-LPs$^{-UV}$ and ICB-LPs$^{+UV}$ in saline (1 mg/mL) for 6 days ($n = 5$). (G) The size of ICB-LPs$^{-UV}$ and ICB-LPs$^{+UV}$ after 0 or 24 h of incubation in mouse serum (1 mg/mL) condition ($n = 5$). (H) Binding kinetics on PD-L1-derivatized biosensors of anti-PD-L1 peptide, PD-L1 mAb and 5 or 10 mol%-incorporated ICB-LPs before and 10 min after UV irradiation. The concentration of anti-PD-L1 peptide, PD-L1 mAb and anti-PD-L1 peptide in each ICB-LPs was unified as 0.067 μmol. (I) The viability of CT26 cells after 48 h of treatment with PEG-LPs, ICB-LPs$^{-UV}$ and ICB-LPs$^{+UV}$ ($n = 5$). Data are presented as mean ± SD ($n = 5$); n.s., $P > 0.05$, $^{***}P < 0.001$ *vs.* Control or indicated.

Fig. S2). Second, the liposomes were placed in a 12-well plate and irradiated with UV lamp (115 V, 60 Hz, 254 nm) for 20 min. The photo-induced crosslinking of $DC_{8,9}PC$ in liposomes have been easily confirmed in the UV−Visible spectrum[19]. The absorption band intensity around 230 nm of liposomes was increased upon UV irradiation in time-dependent manner and it was saturated after 10 min irradiation, indicating that the reaction was completed in a short time of 10 min (Fig. 1B). In addition, the red color of photo-induced cross-linked liposomes (ICB-LPs$^{+UV}$) was clearly observed after 10 min irradiation, compared to ICB-LPs without irradiation (ICB-LPs$^{-UV}$; Fig. 1C). These results show that the 10 min of UV irradiation can fully complete the photo-induced crosslinking of the liposomes and UV irradiation time with 10 min was optimized to prepare the ICB-LPs$^{+UV}$ in our studies.

The average size of ICB-LPs$^{+UV}$ was determined to be 137.7 ± 1.04 nm, which was very similar to that of ICB-LPs$^{-UV}$, indicating that the UV irradiation did not affect on the liposome structure during photo-induced crosslinking polymerization (Fig. 1D). As a control, liposomes in absence of anti-PD-L1 peptide (PEG-LPs), constructed with $DC_{8,9}PC$, DPPC and DSPE-$PEG_{2k}$ at a ratio of 45:45:10 mol%, showed an average size of 105.8 ± 1.23 nm (Supporting Information Table S1). In addition, the zeta potential of ICB-LPs$^{+UV}$ (−3.31 ± 0.219 mV) and ICB-LPs$^{-UV}$ (−2.97 ± 0.175 mV) was almost neutrally charged compared to strongly negatively charged PEG-LPs (−42.2 ± 0.289 mV) owing to modification with positively charged anti-PD-L1 peptide on the liposome surface. TEM images of ICB-LPs$^{-UV}$ and ICB-LPs$^{+UV}$ confirmed a spherical and layered membrane structure of liposome formulation, indicating that the photo-induced crosslinking reaction did not disturb the liposome structure (Fig. 1E). In addition, both ICB-LPs$^{+UV}$ and ICB-LPs$^{-UV}$ were highly stable along with low polydispersity index (PDI) in saline condition, wherein the significant changes in liposome size were not observed for 6 days (Fig. 1F). However, ICB-LPs$^{-UV}$ rapidly aggregated within 24 h of incubation in mouse serum, whereas ICB-LPs$^{+UV}$ efficiently maintained their nanoparticle structures in mouse serum (Fig. 1G). The enhanced serum stability of ICB-LPs$^{+UV}$ is attributable to the intermolecular cross-linking within the liposomal bilayer upon UV irradiation. In addition, their stable particle structures with approximately 137 nm is highly suitable to accumulate within the targeted tumor tissues *via* the EPR effect[20]. Next, biolayer interferometry (BLI) signal of ICB-LPs$^{+UV}$ based on specific interactions with PD-L1 was measured to confirm

PD-L1 multivalent binding mechanism (Fig. 1H). All the ICB-LPs incorporating 5 mol% (5ICB-LPs without or with UV irradiation($^{-/+UV}$) or 10 mol% (10ICB-LPs$^{-/+UV}$) of anti-PD-L1-DSPE-PEG$_{2k}$ showed a stronger PD-L1 binding affinity than anti-PD-L1 peptide and PD-L1 mAb owing to a multivalent binding mechanism. In addition, the PD-L1 binding affinity of 10ICB-LPs$^{-/+UV}$ was significantly enhanced than 5ICB-LPs$^{-/+UV}$. These results are strongly consistent with previous study that demonstrated the optimal density of 10 mol% anti-PD-L1 peptide on the liposome surface to facilitate PD-L1 multivalent binding[23]. Most importantly, each 5ICB-LPs$^{+UV}$ and 10ICB-LPs$^{-UV}$ promoted stronger binding with PD-L1 compared to 5ICB-LPs$^{-UV}$ and 10ICB-LPs$^{+UV}$, respectively. These results indicate that cross-linking of liposome bilayer can enhance the effects of PD-L1 multivalent binding mechanism owing to improved particle stability. Finally, we also assessed the influence of anti-PD-L1-DSPE-PEG$_{2k}$ incorporation on the intrinsic biocompatibility of liposome formulation. As a result, ICB-LPs$^{-UV}$ and ICB-LPs$^{+UV}$ did not induce significant cytotoxicity in CT26 murine colon cancer cells compared to PEG-LPs (Fig. 1I). Collectively, these physicochemical characterization results clearly demonstrate that the ICB-LPs$^{+UV}$ efficiently increase their high serum stability can enhance the PD-L1 target accessibility *via* the nanoparticle-derived passive tumor accumulation owing to the EPR effect *in vivo*.

### 3.2. *Cellular binding and internalization of ICB-LPs$^{+UV}$ in PD-L1 overexpressed tumor cells*

PD-L1 multivalent binding-mediated cellular binding and internalization of ICB-LPs$^{+UV}$were assessed in the PD-L1 overexpressed CT26 murine colon cancer cells. To efficiently monitor the cellular binding and internalization of ICB-LPs$^{+UV}$, methionine deficient green florescent protein-labeled PD-L1-overexpressed CT26 cells (mGFP-CT26 cells) that are prepared by transfection with lentiviral particles encoding mGFP-labeled PD-L1, were employed for in *vitro* experiments. The homogeneous mGFP-labeled PD-L1 expression in the mGFP-CT26 cells was confirmed in previous studies[18]. First, mGFP-CT26 cells were treated with fluorescence dye, APC-labeled PD-L1 mAbs (0.067 μmol) or DiD-labeled ICB-LPs$^{+UV}$ (0.067 μmol based on anti-PD-L1 peptide) for 1 h at 4 °C. The fluorescence images showed that ICB-LPs$^{-UV}$ and ICB-LPs$^{+UV}$ (red color) was mainly observed on the cell surface in similar with PD-L1 mAbs, wherein a strong co-localization (yellow color, white arrow) with mGFP-labeled PD-L1 (green color) was clearly observed (Fig. 2A). In contrast, PEG-LPs (red color) in absence of anti-PD-L1 peptide showed only a little cellular binding in mGFP-CT26 cells, and co-localization with PD-L1 was also not observed. Quantitatively, cellular binding of ICB-LPs$^{-UV}$ and ICB-LPs$^{+UV}$ was nearly similar, which is 1.32−1.44- and 2.11−2.52-fold higher than that of PD-L1 mAbs and PEG-LPs, respectively (Fig. 2B). These enhanced cellular binding of ICB-LPs$^{+UV}$ is attributed to the high PD-L1 multi-binding affinity, as confirmed by BLI analyses. As a control experiment, pre-treatment with PD-L1 mAbs or anti-PD-L1 peptide (NYSKPTDRQYHF) for 1 h at 4 °C to competitively block the PD-L1 on cell membranes significantly decreased the cellular binding of ICB-LPs$^{+UV}$ to the levels of 10.9% and 11.1%, respectively (Fig. 2C and Supporting information Fig. S3). These results indicate that ICB-LPs$^{+UV}$ specifically bind to the PD-L1 receptors on tumor cell surface *via* PD-L1 multivalent-binding mechanism.

Next, the cellular internalization of ICB-LPs$^{+UV}$ into mGFP-CT26 cells was also compared with that of PD-L1 mAbs. Briefly, mGFP-CT26 cells were treated with APC-labeled PD-L1 mAbs or DiD-labeled ICB-LPs$^{+UV}$ for 1 h at 4 °C, and then the cells were further incubated for 12 h at 37 °C after washout of unbound PD-L1 mAbs or ICB-LPs$^{+UV}$. Both APC-labeled PD-L1 mAbs or DiD-labeled ICB-LPs$^{+UV}$ (red color) were observed on the cell membranes immediately after incubation, showing strong co-localization (orange color, white arrow) with PD-L1 (green color; Fig. 2D). In case of PD-L1 mAbs, the co-localization with PD-L1 (orange color) on the cell surface was observed until 3 h of incubation, wherein small amount of PD-L1/PD-L1 mAb complexes (orange color) was endocytosed into the cells. However, those complexes were rapidly dissociated after 6 h of incubation, and only a small amount of PD-L1 mAbs was observed in the mGFP-CT26 cells at 12 h post-incubation. This is because the PD-L1/PD-L1 mAb complexes collapse more easily than PD-L1/PD-1 axis[24]; in addition, the dissociation rates of those complexes are highly accelerated in the acidic endosomes[25]. Therefore, these results show that the PD-L1 mAbs are mostly dissociated from PD-L1 in the cells within 12 h of incubation. As a result, it was clearly observed that green color of PD-L1 was regenerated on the PD-L1 mAb-treated tumor cell surface after 12 h of incubation. In contrast, a large amount of PD-L1/ICB-LPs$^{+UV}$ complexes (orange color, white arrow) was rapidly endocytosed into the cytosol of the cells within 3 h post-incubation. Then, those complexes were sustainably observed in the cells until 12 h post-incubation, indicating that ICB-LPs$^{+UV}$ remained the binding with PD-L1 in the cells without dissociation owing to their stable complex structure by strong PD-L1 binding affinity attributed to the multivalent binding. Quantitatively, over 90% of PD-L1 mAbs was separated from PD-L1 in the tumor cells, whereas approximately 40% of ICB-LPs$^{+UV}$ remained the binding with PD-L1 for 12 h (Fig. 2E). Eventually, PD-L1 (green color) expression in the cells was significantly downregulated after 6 h of incubation. As a control, ICB-LPs$^{-UV}$ also showed a similar intracellular behavior to ICB-LPs$^{+UV}$ after binding with PD-L1 on cell surface. However, amount of PD-L1/ICB-LPs$^{-UV}$ complexes (orange color) within the cells was less compared to those of PD-L1/ICB-LPs$^{+UV}$ because of relatively weak PD-L1 binding affinity. Furthermore, most PD-L1/ICB-LPs$^{-UV}$ complexes were dissociated after 12 h of incubation, wherein only a small amount of ICB-LPs$^{-UV}$ was observed within the cells. These results clearly indicate that PD-L1/ICB-LPs$^{-UV}$ complexes collapsed gradually over time, and ICB-LPs$^{-UV}$ experience lysosomal degradation. These results also demonstrate that PD-L1 multivalent binding of ICB-LPs can significantly enhance the internalization of PD-L1 to the cytoplasm compared with the monovalent binding of PD-L1 mAb. In addition, we have also observed the substantial PD-L1 (green color)/ICB-LPs$^{+UV}$ (red color) complexes in the lysosomes (blue color) after 3 h of incubation, indicating that PD-L1 multivalent binding of ICB-LPs$^{+UV}$ alter subcellular PD-L1 trafficking to deliver it towards to the lysosomes in overlay image (white arrow) (Fig. 2F). In contrast, only small quantity of PD-L1/PD-L1 mAb complexes was localized in the lysosomes at same experimental condition, wherein the lysosomal localization of PD-L1 (10.7%) was also significantly lower compared to tumor cells treated with ICB-LPs$^{+UV}$ for 3 h (41.6%; Fig. 2G). As a control, lysosomal localization of PD-L1 after 3 h of treatment with ICB-LPs$^{-UV}$ was also significantly lower than ICB-LPs$^{+UV}$ as levels of 30.1%. This is attributable to that PD-L1 prone to enter the recycling endosomes instead of lysosomes after conformational binding with PD-L1 mAbs[9]. Taken together, the ICB-LPs$^{+UV}$ efficiently promotes the internalization and lysosomal delivery of PD-L1 *via* PD-L1 multivalent binding.

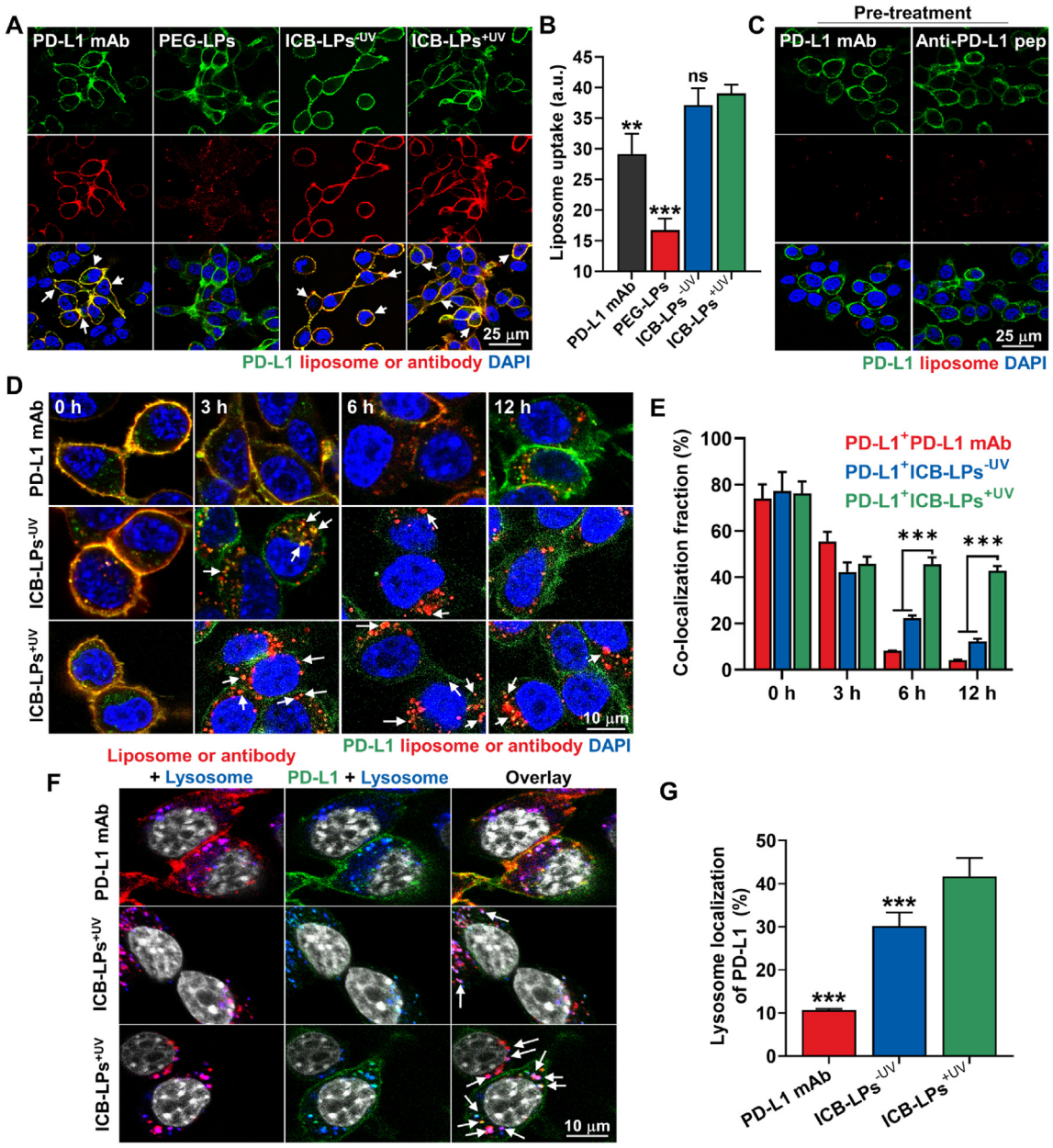


**Figure 2** Cellular binding and internalization of ICB-LPs$^{+UV}$. (A) The cellular binding of PD-L1 mAbs, PEG-LPs, ICB-LPs$^{-UV}$ and ICB-LPs$^{+UV}$ in mGFP-CT26 cells 1 h post-incubation at 4 °C. Equivalent lipid concentration of PEG-LPs was treated in cells. (B) Quantitative analyses for the cellular binding of PD-L1 mAbs, PEG-LPs, ICB-LPs$^{-UV}$ and ICB-LPs$^{+UV}$ in mGFP-CT26 cells 1 h post-incubation at 4 °C. The concentration of PD-L1 mAb and anti-PD-L1 peptide in ICB-LPs was unified as 0.067 μmol. Fluorescence (red color) in the images was quantified *via* the ImageJ software. (C) The cellular binding of ICB-LPs$^{+UV}$ after 1 h of treatment at 4 °C in the mGFP-CT26 cells pre-treated with PD-L1 mAbs or peptide for 24 h. (D) The cellular uptake of PD-L1 mAbs, ICB-LPs$^{-UV}$ and ICB-LPs$^{+UV}$ after binding with PD-L1 in mGFP-CT26 cells for 0, 3, 6 or 12 h. The concentration of PD-L1 mAb and anti-PD-L1 peptide in ICB-LPs was unified as 0.067 μmol/L. (E) Quantitative analyses for co-localization of PD-L1 mAbs, ICB-LPs$^{-UV}$ or ICB-LPs$^{+UV}$ with the PD-L1 in the mGFP-CT26 cells. Fluorescence (orange color) in the images was quantified *via* the ImageJ software. (F) Lysosomal localization of PD-L1 mAbs, ICB-LPs$^{-UV}$ or ICB-LPs$^{+UV}$ in mGFP-CT26 cells after 3 h of treatment. (G) Quantitative analyses for the amount of PD-L1 mAbs, ICB-LPs$^{-UV}$, ICB-LPs$^{+UV}$ and PD-L1 in the lysosomes were performed *via* the ImageJ software. Data are presented as mean ± SD ($n = 5$); ***$P < 0.001$ *vs.* Control or indicated.

### *3.3. Lysosomal PD-L1 degradation and T cell-mediated immune responses of ICB-LPs$^{+UV}$*

The effective lysosomal PD-L1 degradation by PD-L1 multivalent binding of ICB-LPs$^{+UV}$ was evaluated in mGFP-CT26 cells after treatment with PD-L1 mAbs (0.067 μmol) or ICB-LPs$^{+UV}$ (0.067 μmol based on anti-PD-L1 peptide) for 72 h at 37 °C (Fig. 3A). In case of PD-L1 mAb-treated mGFP-CT26 cells, mGFP-labeled PD-L1 (green color) on the cell surface was significantly decreased until 6 h of incubation, but that was rapidly regenerated from 9 h post-incubation. These results indicate that PD-L1 mAb-induced PD-L1 blockade results in PD-L1 recycling owing to rapid dissociation of PD-L1 mAbs from PD-L1 and its subcellular fate that enters into the recycling endosomes[9,24,25]. In

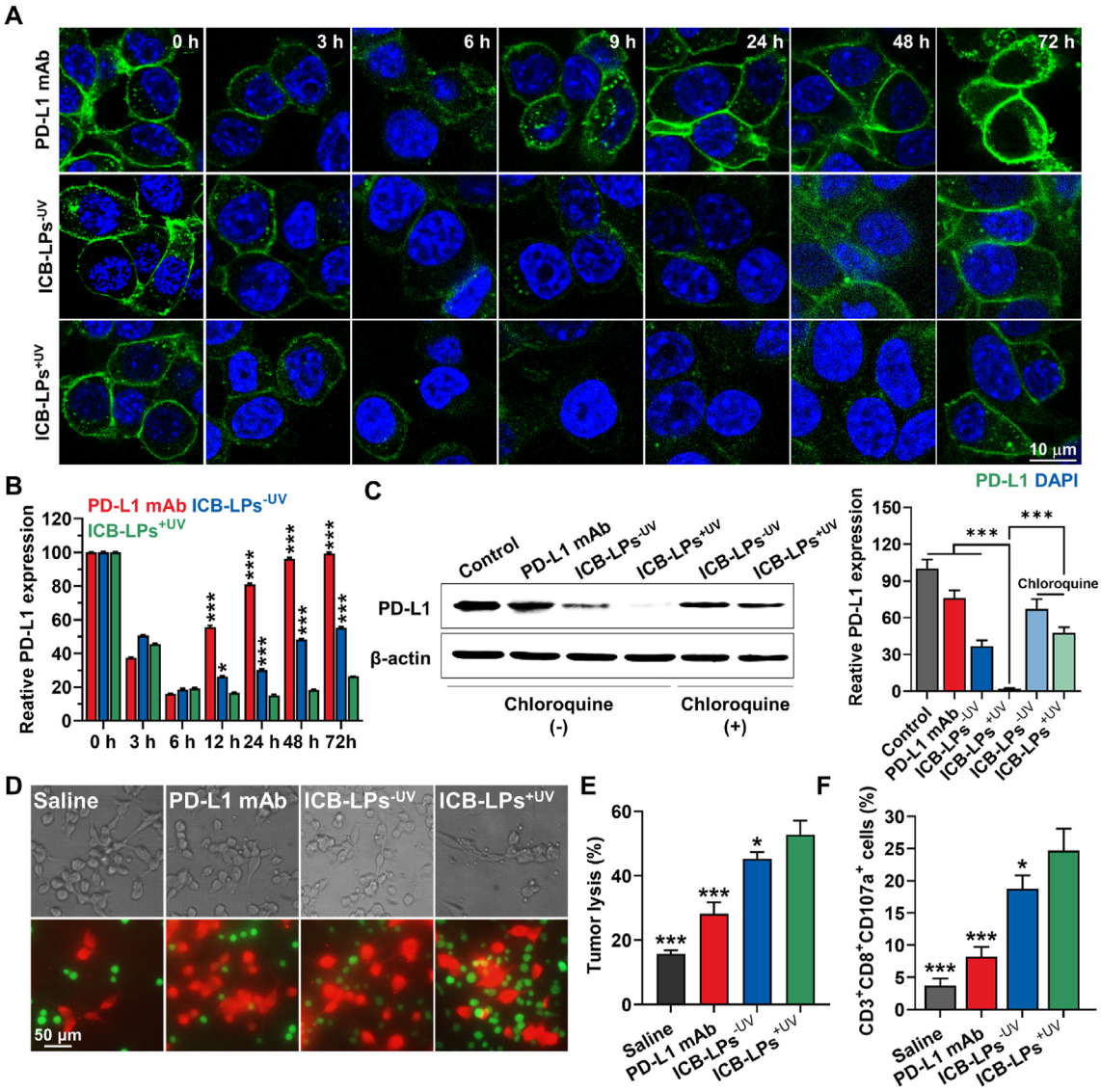


**Figure 3** Lysosomal PD-L1 degradation and T cell-mediated antitumor immune responses by ICB-LPs$^{+UV}$. (A) Expression of PD-L1 in mGFP-CT26 cells after treatment with PD-L1 mAbs, ICB-LPs$^{-UV}$ or ICB-LPs$^{+UV}$. The concentration of PD-L1 mAb and anti-PD-L1 peptide in ICB-LPs was unified as 0.067 μmol. (B) Quantitative analyses for the amount of PD-L1 in mGFP-CT26 cells after treatment with PD-L1 mAbs, ICB-LPs$^{-UV}$ or ICB-LPs$^{+UV}$. Fluorescence (green color) in the images was quantified *via* the ImageJ software. (C) Western blot analyses showing PD-L1 expression in the mGFP-CT26 cells after treatment with PD-L1 mAbs, ICB-LPs$^{-UV}$ or ICB-LPs$^{+UV}$ for 48 h. As a control, PD-L1 expression in the mGFP-CT26 cells pre-treated with chloroquine (100 μmol) for 24 h was assessed after treatment with ICB-LPs$^{-UV}$ and ICB-LPs$^{+UV}$ for 48 h. (D) The optical and fluorescence images of $CD8^+$ T cells co-cultured with CT26 cells pre-treated with PD-L1 mAbs, ICB-LPs$^{-UV}$ or ICB-LPs$^{+UV}$ for 24 h. (E) The tumor cell lysis after co-culture of $CD8^+$ T cells with CT26 cells pre-treated with PD-L1 mAbs, ICB-LPs$^{-UV}$ or ICB-LPs$^{+UV}$ for 24 h. (F) The CD107a exposure on the $CD8^+$ T cells after co-culture with CT26 cells pre-treated with PD-L1 mAbs, ICB-LPs$^{-UV}$ or ICB-LPs$^{+UV}$ for 24 h. Data are presented as mean ± SD ($n = 5$); $^*P < 0.05$, $^{***}P < 0.001$ *vs.* Control or indicated.

contrast, ICB-LPs$^{+UV}$ induced durable PD-L1 degradation in the mGFP-CT26 cells; approximately 90% of PD-L1 disappeared in the tumor cells, whereas over 80% of PD-L1 was regenerated after 24 h of PD-L1 mAb treatment (Fig. 3B). These effective PD-L1 degradation by ICB-LPs$^{+UV}$ sustainably retained for 48 h of incubation, and certain PD-L1 levels were regenerated at 72 h post-incubation. As a control, ICB-LPs$^{-UV}$ also promoted an effective PD-L1 degradation in mGFP-CT26 cells, but PD-L1 within the cells was gradually repopulated from 9 h post-incubation. These results are attributable to intracellular behaviors of ICB-LPs$^{-UV}$ that experience lysosomal degradation after dissociation from PD-L1 after 6 h of incubation due to a relatively weak PD-L1 binding affinity, as shown in Fig. 2D. A significant decrease in the cellular PD-L1 abundance by multivalent binding-mediated lysosomal PD-L1 delivery was additionally confirmed using Western blot analysis. It was confirmed that the PD-L1 expression levels of ICB-LPs$^{+UV}$-treated CT26 cells were reduced by 2.6 ± 0.27% and 5.56 ± 0.81%, compared to the PD-L1 mAbs- or ICB-LPs$^{-UV}$-treated CT26 cells, respectively (Fig. 3C). Furthermore, the effects of multivalent binding-mediated lysosomal PD-L1 degradation by ICB-LPs were significantly reduced when the CT26 cells were pre-treated with inhibitor of lysosomal pathway of protein degradation, chloroquine (100 μmol/L) for 24 h, which directly demonstrates that ICB-LPs$^{+UV}$ promote efficient PD-L1

degradation *via* multivalent binding-mediated lysosomal PD-L1 delivery[26]. These results demonstrate that multivalent binding of ICB-LPs$^{+UV}$ to PD-L1 overexpressed cancer cells can promote durable and reliable PD-L1 degradation by delivering overexpressed PD-L1 on the cell membranes to the lysosomes instead of recycling endosomes, compared to PD-L1 mAbs.

Next, we performed co-culture assays to evaluate whether ICB-LPs$^{+UV}$ can significantly enhance the T cell-mediated antitumor immune responses owing to their multivalent binding-mediated effective and durable lysosomal PD-L1 degradation. Briefly, CD8$^+$ T cells were collected from the lymph nodes and spleen of BALB/c mice and then activated with the anti-CD28 antibodies on the cell culture plate coated with the anti-CD3 antibodies[27]. When the CT26 cells ($2 \times 10^5$; red color) pre-treated with PD-L1 mAbs (0.067 μmol), ICB-LPs$^{-UV}$ or ICB-LPs$^{+UV}$ (0.067 μmol based on anti-PD-L1 peptide) were co-cultured with CD8$^+$ T cells ($1 \times 10^6$; green color) for 1 h at 37 °C, the number of CD8$^+$ T cells (green color; CFSE) bound to ICB-LPs$^{+UV}$-treated tumor cells (red color; CellTracker™) was significantly increased than those treated with PD-L1 mAbs or ICB-LPs$^{-UV}$ (Fig. 3D). These results show an enhanced target recognition of T cells owing to the effective blockade of the PD-1/PD-L1 axis by the effective and durable PD-L1 degradation of ICB-LPs$^{+UV}$. As a result, tumor cell lysis was significantly elevated after treatment of CT26 cells with ICB-LPs$^{+UV}$ compared to PD-L1 mAbs and ICB-LPs$^{-UV}$ when the tumor cells were co-cultured with CD8$^+$ T cells at a 5:1 (effector to target) ratio (Fig. 3E). Finally, higher CD107a expressions on CD8$^+$ T cells were clearly observed after co-culture with the CT26 cells treated with ICB-LPs$^{+UV}$ than other groups, indicating T cell degranulation by target recognition (Fig. 3F). These results show that ICB-LPs$^{+UV}$ promotes effective and durable PD-L1 degradation *via* multivalent binding-mediated lysosomal PD-L1 degradation and subsequently blocks PD-1/PD-L1 axis, thereby enhancing T cell-mediated antitumor immune responses in cultured cells.

### 3.4. *In vivo tumor targeting and effective PD-L1 degradation of ICB-LPs$^{+UV}$ in tumor bearing mice*

To assess improved biodistribution and tumor targeting of ICB-LPs$^{+UV}$, their pharmacokinetics (PK) profiles were compared to PEG-LPs and ICB-LPs$^{-UV}$ in BALB/c mice. For this analysis, 1 mg/kg of DiD-labeled PEG-LPs, ICB-LPs$^{-UV}$ and ICB-LPs$^{+UV}$ was intravenously injected in the mice, followed by collection of blood samples at pre-determined times. Interestingly, PEG-LPs showed relatively rapid *in vivo* clearance with a short half-life ($t_{1/2}$) of 4.12 ± 0.42 h, whereas ICB-LPs$^{-UV}$ exhibited a significantly prolonged $t_{1/2}$ of 6.55 ± 1.1 h (Fig. 4A and Supporting Inforamtion Table S2). Importantly, ICB-LPs$^{+UV}$ exhibited a greatly extended $t_{1/2}$ of 18.3 ± 2.1 h with 2.37−2.58- and 1.54−1.7-fold higher area under the curves (AUC) than PEG-LPs and ICB-LPs$^{-UV}$, respectively. These results are attributable to the improved particle stability by cross-linking of liposomal bilayers after UV irradiation. In addition, a detectable, ICB-LPs$^{+UV}$ remained for 72 h in the body, showing a significantly extended residence time *in vivo*. Motivated by the greatly improved PK profiles of ICB-LPs$^{+UV}$, the tumor targeting efficiency of DiD-labeled ICB-LPs$^{+UV}$ was assessed in CT26 colon tumor-bearing mice, which were prepared by subcutaneous inoculation of $1 \times 10^6$ CT26 cells into the flank of BALB/c mice. When the colon tumor volumes were approximately 200 mm$^3$, an equivalent dose (1 mg/kg) of DiD-labeled PEG-LPs, ICB-LPs$^{-UV}$ or ICB-LPs$^{+UV}$ was intravenously administered into the mice. First, NIRF imaging results showed that the PEG-LPs considerably accumulated within the targeted tumor tissues after 24 h of injection owing to nanoparticle-derived EPR effect (Fig. 4B). Interestingly, ICB-LPs$^{-UV}$ exhibited the higher tumor accumulation compared with PEG-LPs, which is attributable to the PD-L1 receptor-mediated active tumor targeting in addition to the passive tumor targeting of PEGylated liposomes[20]. Notably, a highest tumor accumulation of ICB-LPs$^{+UV}$ was clearly observed in the colon tumor-bearing mice, showing 1.99−2.11- and 1.31−1.4-fold strong fluorescence signals in tumor region compared to PEG-LPs and ICB-LPs$^{-UV}$, respectively (Fig. 4C). These results demonstrate that the photo-induced crosslinked ICB-LPs$^{+UV}$ can promote the multivalent binding with PD-L1, and their high serum stability can enhance the PD-L1 target accessibility *via* the nanoparticle-derived passive tumor accumulation, compared to other liposome formulations.

The *ex vivo* fluorescence imaging of major organs and tumor tissues further showed a significantly high tumor accumulation of ICB-LPs$^{+UV}$ after 24 h of injection, wherein the fluorescence intensities in the tumors were 2.03−2.11- and 1.34−1.42-fold stronger than those of PEG-LPs and ICB-LPs$^{-UV}$, respectively (Fig. 4D). This considerable tumor accumulation of ICB-LPs$^{+UV}$ is attributed to the enhanced passive and active tumor targeting owing to a high stability in the blood stream by crosslinked liposome formulation[19]. Histological analyses also showed a significant accumulation of ICB-LPs$^{+UV}$ (red color) in the tumor tissues compared with PEG-LPs and ICB-LPs$^{-UV}$ at 24 h post-injection (Fig. 4E). Finally, the effective *in vivo* PD-L1 degradation by multivalent binding-mediated lysosomal PD-L1 degradation was further investigated *via* Western blot analysis, wherein the PD-L1 expression levels in tumor tissues were significantly downregulated to 31.7 ± 2.23% and 52.3 ± 4.01% after 24 h of treatment with ICB-LPs$^{+UV}$ compared with PEG-LPs and ICB-LPs$^{-UV}$, respectively (Fig. 4F). Taken together, ICB-LPs$^{+UV}$ highly accumulates within the tumor tissues *via* both passive and active targeting based on high stability of crosslinked liposome formulation for target access and promotes effective *in vivo* PD-L1 degradation *via* multivalent binding-mediated lysosomal PD-L1 degradation mechanism.

### 3.5. *Antitumor efficacy and immune responses of ICB-LPs$^{+UV}$ in tumor bearing mice*

The antitumor efficacy and immune responses of ICB-LPs$^{+UV}$ were assessed in colon tumor models. Briefly, the mice were randomly divided into four groups when the tumor volumes were approximately 50−60 mm$^3$; then, saline, PD-L1 mAbs (10 mg/kg), or equivalent 1 mg/kg dose of ICB-LPs$^{-UV}$ or ICB-LPs$^{+UV}$ were intravenously injected into the mice once every 3 days. As expected, the mice treated with ICB-LPs$^{+UV}$ (463.03 ± 145.17 mm$^3$) exhibited a significantly inhibited tumor growth on Day 13 after treatment compared with saline (1813.4 ± 280.55 mm$^3$), PD-L1 mAbs (1106.68 ± 173.6 mm$^3$) and ICB-LPs$^{-UV}$ (905.84 ± 264.87 mm$^3$) groups, respectively (Fig. 5A). In addition, histological analyses of tumor tissues clearly showed a significant apoptotic cell death along with PD-L1 downregulation in ICB-LPs$^{+UV}$-treated mice compared to other groups on Day 13, thereby showing the potent antitumor efficacy by efficient PD-L1 degradation owing to multivalent binding-mediated lysosomal PD-L1 degradation *in vivo* (Fig. 5B and Supporting Information Fig. S4). With intrinsic biocompatibility of liposome formulation, significant systemic toxicities were not observed in the mice

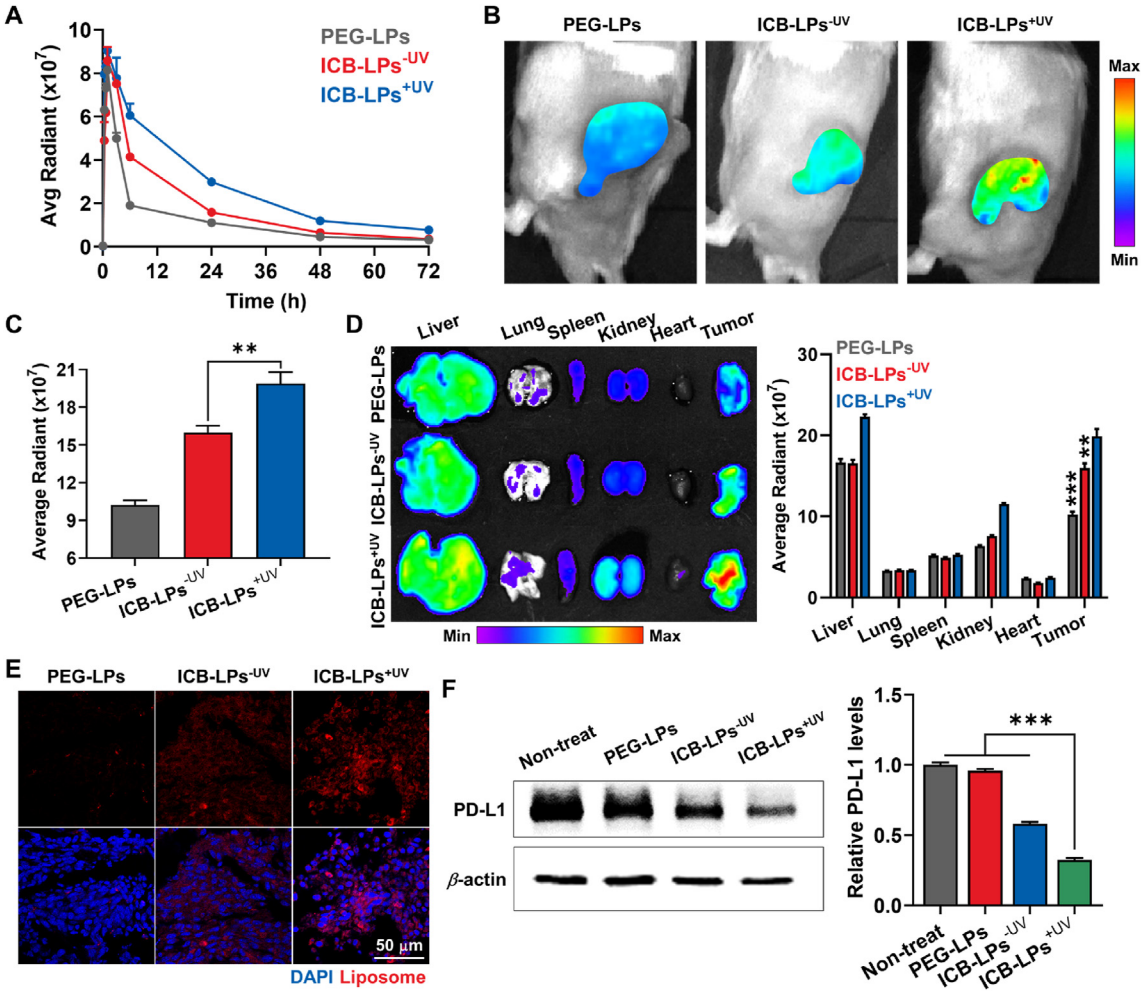


**Figure 4** *In vivo* tumor targeting and PD-L1 degradation by ICB-LPs$^{+UV}$. (A) Time-dependent serum concentration of PEG-LPs, ICB-LPs$^{-UV}$ or ICB-LPs$^{+UV}$ after intravenous injection with equivalent 1 mg/kg dose in BALB/c mice ($n = 3$). Fluorescence intensities in serum were quantified using Living Image software. (B) NIRF images of CT26 colon tumor-bearing mice treated with equivalent 1 mg/kg dose of PEG-LPs, ICB-LPs$^{-UV}$ or ICB-LPs$^{+UV}$ after 24 h of injection. Fluorescence intensities in tumor regions were quantified using Living Image software. (C) Quantitative analyses for the fluorescence intensities in the tumor regions after 24 h of injection of PEG-LPs, ICB-LPs$^{-UV}$ or ICB-LPs$^{+UV}$ ($n = 3$). (D) *Ex vivo* NIRF images of major organs and tumor tissues collected from mice treated with PEG-LPs, ICB-LPs$^{-UV}$ or ICB-LPs$^{+UV}$ after 24 h of injection ($n = 3$). (E) Quantitative analyses for the fluorescence intensities in the major organs and tumor tissues after 24 h of injection of PEG-LPs, ICB-LPs$^{-UV}$ or ICB-LPs$^{+UV}$. (F) Histology of tumor tissues after 24 h of injection of PEG-LPs, ICB-LPs$^{-UV}$ or ICB-LPs$^{+UV}$ ($n = 3$). (G) Western blot analyses showing PD-L1 expression in the tumor tissues after 24 h of treatment with PEG-LPs, ICB-LPs$^{-UV}$ or ICB-LPs$^{+UV}$. PD-L1 band intensity in Western blot image was quantified *via* the ImageJ software. Data are presented as mean ± SD ($n = 3$); $^{***}P < 0.001$ *vs.* Control or indicated.

treated with ICB-LPs$^{+UV}$, wherein the body weight changes were similar with saline and other groups during treatments (Fig. 5C). Importantly, the median survival of the mice in the saline, PD-L1 mAb and ICB-LPs$^{-UV}$ groups was determined to be 16, 16 and 17 days, respectively, and the mice were dead owing to the tumor progression (Fig. 5D). In contrast, ICB-LPs$^{+UV}$-treated mice were survived for over 20 days with a significantly inhibited tumor growth. Next, the CTLs ($CD45^+CD3^+CD8^+$) and regulatory T cells (Treg; $CD3^+CD4^+CD25^+$) in the tumor tissues were analyzed after 13 days of treatment to evaluate the antitumor immune responses by ICB-LPs$^{+UV}$. As expected, the proportion of CTLs in the tumor tissues was 2.31−2.44- and 2.51−2.66-fold higher in mice treated with ICB-LPs$^{+UV}$ than in those treated with PD-L1 mAbs and ICB-LPs$^{-UV}$, respectively (Fig. 5E and Supporting Information Fig. S5A). In addition, the levels of granzyme B (GrzB)-secreting $CD8^+$ T cells were upregulated 3.41−3.66-, 1.89−2.01- and 1.78−1.95-fold in ICB-LPs$^{+UV}$ group than saline, PD-L1 mAbs and ICB-LPs$^{-UV}$ groups, indicating a high activity of CTLs (Fig. 5F and S7B). The high CTL activity in the tumor tissues of the ICB-LPs$^{+UV}$ group was further confirmed by measuring the elevated quantities of IFN-γ, which is released from activated T cells in the tumor microenvironment (Fig. 5G). These results indicate an increase in the numbers and activities of tumor-infiltrating CTLs by multivalent binding-mediated *in vivo* PD-L1 degradation that enhances the target recognition. Finally, Tregs in the tumor tissues were considerably downregulated in the ICB-LPs$^{+UV}$ group compared with the other groups, resulting in significantly increased ratio of CTLs to Tregs in the tumor tissues (Fig. 5H and S7C). A significant antitumor efficacy of ICB-LPs$^{+UV}$ was also observed in the 4T1 breast tumor models that

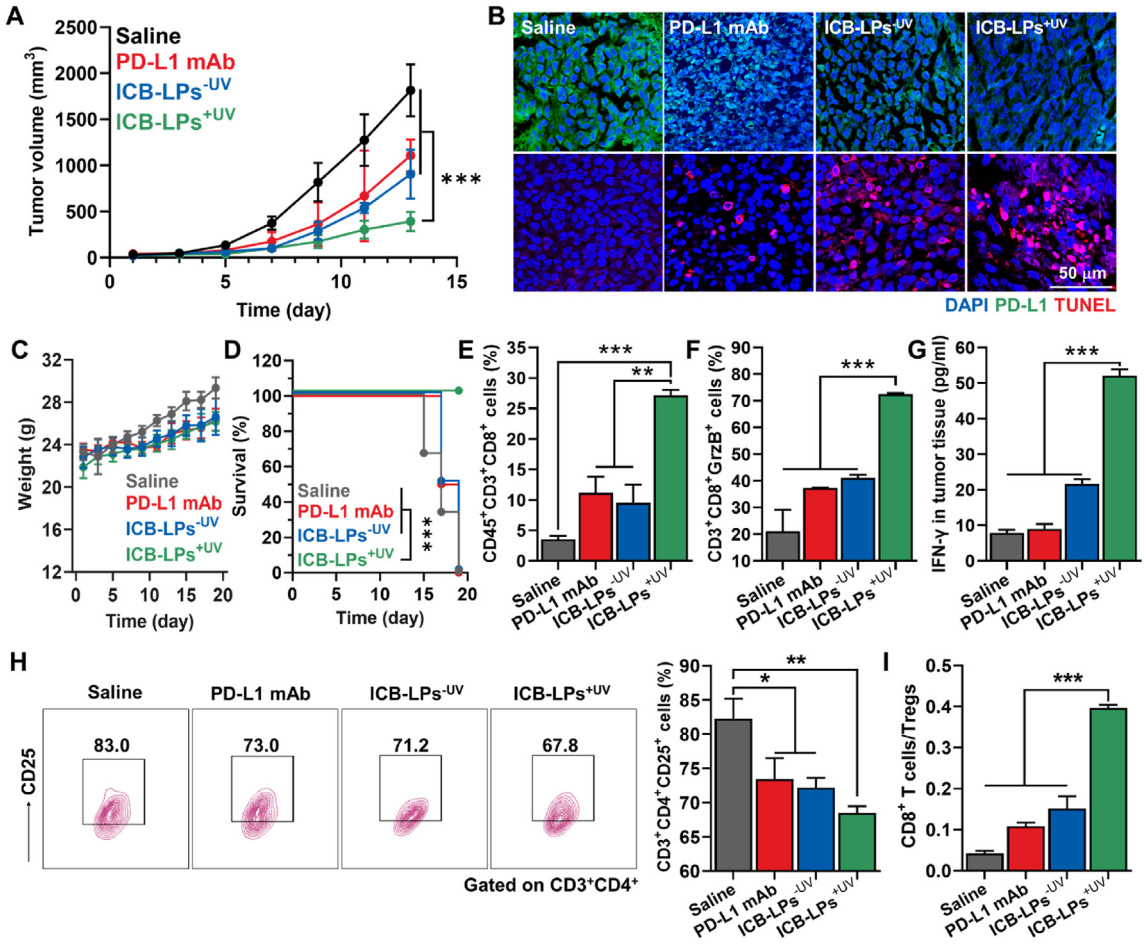


**Figure 5** Antitumor efficacy and immune responses of ICB-LPs$^{+UV}$. (A) Tumor growth of CT26 colon tumor-bearing mice during treatment ($n = 5$). Saline, PD-L1 mAbs (10 mg/kg), or equivalent 1 mg/kg dose of ICB-LPs$^{-UV}$ or ICB-LPs$^{+UV}$ were intravenously injected into the mice once every 3 days. (B) Tumor tissues stained with APC-conjugated anti-PD-L1 antibody or TUNEL on Day 18 after treatment with saline, PD-L1 mAbs, ICB-LPs$^{-UV}$ or ICB-LPs$^{+UV}$. (C) Body weight changes of mice during treatment with saline, PD-L1 mAbs, ICB-LPs$^{-UV}$ or ICB-LPs$^{+UV}$ once every three days ($n = 5$). (D) Mice survival during treatment with saline, PD-L1 mAbs, ICB-LPs$^{-UV}$ or ICB-LPs$^{+UV}$ once every three days ($n = 5$). Survival data was plotted as Kaplan−Meier curves and analyzed using log-rank test. (E and F) The population of (E) CTLs ($CD45^+CD3^+CD8^+$) and (F) granzyme B (GrzB)-secreting $CD8^+$ T cells in the tumor tissues after 18 days of treatment with saline, PD-L1 mAbs, ICB-LPs$^{-UV}$ or ICB-LPs$^{+UV}$ ($n = 5$). (G) IFN-γ in the tumor supernatants after 18 days of treatment with saline, PD-L1 mAbs, ICB-LPs$^{-UV}$ or ICB-LPs$^{+UV}$ ($n = 5$). (H) The population of Tregs ($CD3^+CD4^+CD25^+$) in the tumor tissues after 18 days of treatment with saline, PD-L1 mAbs, ICB-LPs$^{-UV}$ or ICB-LPs$^{+UV}$ ($n = 5$). (I) The ratio of CTLs to Tregs in the tumor tissues after 18 days of treatment with saline, PD-L1 mAbs, ICB-LPs$^{-UV}$ or ICB-LPs$^{+UV}$ ($n = 5$). Data are presented as mean ± SD ($n = 5$); n.s., $P > 0.05$, $^*P < 0.05$, $^{**}P < 0.01$, $^{***}P < 0.001$ *vs.* Control or indicated.

are poorly immunogenic and highly metastatic in contrast to highly immunogenic CT26 colon tumor models (Supporting Information Fig. S8)[28]. Treatment with ICB-LPs$^{+UV}$ significantly increased the CTLs and excluded Tregs within the 4T1 tumor tissues *via* efficient multivalent binding-mediated PD-L1 degradation, thereby greatly inhibiting tumor growth compared to PD-L1 mAbs and ICB-LPs$^{-UV}$. Taken together, ICB-LPs$^{+UV}$ significantly inhibits the tumor progression by recruiting a large number of tumor-infiltrating CTLs and excluding the Tregs at the targeted tumor tissues *via* the effective PD-L1 degradation through the multivalent binding-mediated lysosomal degradation of ICB-LPs$^{+UV}$.

## 4. Conclusions

In this study, we proposed photo-induced crosslinked and anti-PD-L1 peptide incorporated liposomes to promote PD-L1 multivalent binding for effective immune checkpoint blockade therapy. First, liposome formulation was constructed with $DC_{8,9}PC$ of photo-polymerized diacetylenic moiety, DPPC and PD-L1-DSPE-$PEG_2$ in a molar ratio of 45:45:10, followed by cross-linking of liposomal bilayer upon UV irradiation for 10 min. The resulting ICB-LPs$^{+UV}$ showed highly stable spherical and layered membrane structure of liposome formulation. Importantly, the ICB-LPs$^{+UV}$ promoted the multivalent binding with PD-L1 on the tumor cell surface, which delivered PD-L1 to the lysosomes; this was clearly different from intracellular fate of PD-L1 targeting recycling endosomes after binding with PD-L1 mAbs. As a result, ICB-LPs$^{+UV}$ efficiently downregulated the PD-L1 levels in tumor cells *via* multivalent binding-mediated lysosomal PD-L1 degradation, resulting in reinvigoration effect of CTLs in - studies. When the ICB-LPs$^{+UV}$ were intravenously administered in the colon tumor-bearing mice, they highly accumulated within the targeted tumor tissues by passive and active tumor targeting mechanisms, inducing a potent immune checkpoint blockade

therapy premised on the effective and durable PD-L1 degradation. Collectively, this study demonstrated the superior antitumor efficacy of photo-induced crosslinked and anti-PD-L1 peptide-incorporated liposome formulation that promotes PD-L1 multivalent binding for its trafficking toward the lysosomes instead of the recycling endosomes.

## Acknowledgments

This work was supported by grants from the National Research Foundation (NRF) of Korea, funded by the Ministry of Science (NRF-2022M3H4A1A03067401 and NRF-2021R1C1C2005460, Republic of Korea) and the Intramural Research Program of KIST.

## Author contributions

Youngjoo Lee: Validation, Formal analysis, Investigation, Data curation, Visualization., Sukyung Song: Validation, Formal analysis, Investigation, Data curation, Visualization., Suah Yang: Methodology, Investigation., Jinseong Kim: Investigation., Yujeong Moon: Investigation., Nayeon Shim: Investigation., Hong Yeol Yoon: Methodology., Sehoon Kim: Methodology., Man Kyu Shim: Conceptualization, Methodology, Formal analysis, Data curation, Funding acquisition, Writing-Original Draft, Writing - Review & Editing., Kwangmeyung Kim: Conceptualization, Resources, Supervision, Funding acquisition, Project administration, Writing-Original Draft, Writing - Review & Editing.

## Conflicts of interest

The authors declare no conflicts of interest.

## Appendix A. Supporting information

Supporting data to this article can be found online at https://doi.org/10.1016/j.apsb.2023.09.007.

## References

1. Savoldo B, Rooney CM, Di Stasi A, Abken H, Hombach A, Foster AE, et al. Epstein Barr virus−specific cytotoxic T lymphocytes expressing the anti-CD30ζ artificial chimeric T-cell receptor for immunotherapy of Hodgkin disease. *Blood* 2007;**110**:2620−30.
2. Wei SC, Duffy CR, Allison JP. Fundamental mechanisms of immune checkpoint blockade therapy. *Cancer Discov* 2018;**8**:1069−86.
3. Postow MA, Callahan MK, Wolchok JD. Immune checkpoint blockade in cancer therapy. *J Clin Oncol* 2015;**33**:1974−82.
4. Jorgovanovic D, Song M, Wang L, Zhang Y. Roles of IFN-γ in tumor progression and regression: a review. *Biomark Res* 2020;**8**:49.
5. Cha JH, Chan LC, Li CW, Hsu JL, Hung MC. Mechanisms controlling PD-L1 expression in cancer. *Mol Cell* 2019;**76**:359−70.
6. Armand P. Immune checkpoint blockade in hematologic malignancies. *Blood* 2015;**125**:3393−400.
7. Kubli SP, Berger T, Araujo DV, Siu LL, Mak TW. Beyond immune checkpoint blockade: emerging immunological strategies. *Nat Rev Drug Discov* 2021;**20**:899−919.
8. Kalbasi A, Ribas A. Tumour-intrinsic resistance to immune checkpoint blockade. *Nat Rev Immunol* 2020;**20**:25−39.
9. Li L, Li Y, Yang CH, Radford DC, Wang J, Janát-Amsbury M, et al. Inhibition of immunosuppressive tumors by polymer-assisted inductions of immunogenic cell death and multivalent PD-L1 crosslinking. *Adv Funct Mater* 2020;**30**:1908961.
10. Burr ML, Sparbier CE, Chan Y-C, Williamson JC, Woods K, Beavis PA, et al. CMTM6 maintains the expression of PD-L1 and regulates anti-tumour immunity. *Nature* 2017;**549**:101−5.
11. Ren Y, Qian Y, Ai L, Xie Y, Gao Y, Zhuang Z, et al. TRAPPC4 regulates the intracellular trafficking of PD-L1 and antitumor immunity. *Nat Commun* 2021;**12**:1−15.
12. Wang H, Yao H, Li C, Shi H, Lan J, Li Z, et al. HIP1R targets PD-L1 to lysosomal degradation to alter T cell-mediated cytotoxicity. *Nat Chem Biol* 2019;**15**:42−50.
13. Moody PR, Sayers EJ, Magnusson JP, Alexander C, Borri P, Watson P, et al. Receptor crosslinking: a general method to trigger internalization and lysosomal targeting of therapeutic receptor: ligand complexes. *Mol Ther* 2015;**23**:1888−98.
14. Wang Q, Villeneuve G, Wang Z. Control of epidermal growth factor receptor endocytosis by receptor dimerization, rather than receptor kinase activation. *EMBO Rep* 2005;**6**:942−8.
15. Lee CW, Zhang H, Geng L, Peng HB. Crosslinking-induced endocytosis of acetylcholine receptors by quantum dots. *PLoS One* 2014;**9**:e90187.
16. Weflen AW, Baier N, Tang Q-J, Van den Hof M, Blumberg RS, Lencer WI, et al. Multivalent immune complexes divert FcRn to lysosomes by exclusion from recycling sorting tubules. *Mol Biol Cell* 2013;**24**:2398−405.
17. Bu J, Nair A, Iida M, Jeong WJ, Poellmann MJ, Mudd K, et al. An avidity-based PD-L1 antagonist using nanoparticle-antibody conjugates for enhanced immunotherapy. *Nano Lett* 2020;**20**:4901−9.
18. Yang S, Shim MK, Song S, Cho H, Choi J, Jeon SI, et al. Liposome-mediated PD-L1 multivalent binding promotes the lysosomal degradation of PD-L1 for T cell-mediated antitumor immunity. *Biomaterials* 2022;**290**:121841.
19. Callens M, Beltrami M, D'Agostino E, Pfeiffer H, Verellen D, Paradossi G, et al. The photopolymerization of $DC_{8,\ 9}PC$ in microbubbles. *Colloids Surf A Physicochem Eng Asp* 2019;**568**:371−80.
20. Bertrand N, Wu J, Xu X, Kamaly N, Farokhzad OC. Cancer nanotechnology: the impact of passive and active targeting in the era of modern cancer biology. *Adv Drug Deliv Rev* 2014;**66**:2−25.
21. Moon Y, Shim MK, Choi J, Yang S, Kim J, Yun WS, et al. Anti-PD-L1 peptide-conjugated prodrug nanoparticles for targeted cancer immunotherapy combining PD-L1 blockade with immunogenic cell death. *Theranostics* 2022;**12**:1999.
22. Chang HN, Liu BY, Qi YK, Zhou Y, Chen YP, Pan KM, et al. Blocking of the PD-1/PD-L1 interaction by ad-peptide antagonist for cancer immunotherapy. *Angew Chem Int Ed Engl* 2015;**54**:11760−4.
23. Yang S, Shim MK, Song S, Cho H, Choi J, Jeon SI, et al. Liposome-mediated PD-L1 multivalent binding promotes the lysosomal degradation of PD-L1 for T cell-mediated antitumor immunity. *Biomaterials* 2022;**290**:121841.
24. Qin J, Zhang M, Guan Y, Guo X, Li Z, Rankl C, et al. Imaging and quantifying analysis the binding behavior of PD-L1 at molecular resolution by atomic force microscopy. *Anal Chim Acta* 2022;**1191**:339281.
25. Liu H, Bi X, Zhou Y, Shi R, Yao S, Qi J, et al. Identification of a hotspot on PD-L1 for pH-dependent binding by monoclonal antibodies for tumor therapy. *Signal Transduct Targeted Ther* 2020;**5**:1−3.
26. Seglen PO, Grinde B, Solheim AE. Inhibition of the lysosomal pathway of protein degradation in isolated rat hepatocytes by ammonia, methylamine, chloroquine and leupeptin. *European J Mol Biol* 1979;**95**:215−25.
27. Jeon IS, Yoo JD, Gurung S, Kim M, Lee C, Park EJ, et al. Anticancer nanocage platforms for combined immunotherapy designed to harness immune checkpoints and deliver anticancer drugs. *Biomaterials* 2021;**270**:120685.
28. Kim K, Skora AD, Li Z, Liu Q, Tam AJ, Blosser RL, et al. Eradication of metastatic mouse cancers resistant to immune checkpoint blockade by suppression of myeloid-derived cells. *Proc Natl Acad Sci U S A* 2014;**111**:11774−9.